https://doi.org/10.5194/wes-2019-105
Preprint. Discussion started: 28 January 2020

eawe european academy of wind energy
Open Access WIND ENERGY SCIENCE DISCUSSIONS

Should wind turbines rotate in the opposite direction?

Antonia Englberger[1], Julie K. Lundquist[2,3], and Andreas Dörnbrack[1]

[1]German Aerospace Center, Institute of Atmospheric Physics, Oberpfaffenhofen, Germany
[2]Department of Atmospheric and Oceanic Sciences, University of Colorado Boulder, Boulder, USA
[3]National Renewable Energy Laboratory, Golden, Colorado, USA

Correspondence: Antonia Englberger (antonia.englberger@dlr.de)

Abstract. Wind turbine blades rotate in clockwise direction seeing from an upstream position. This rotational direction impacts the wake in a stably stratified atmospheric boundary layer, in which the wind profile is characterised by a veering or a backing wind. Here, we challenge the arbitrary choice of the rotational direction of the blades by investigating the interaction of the rotational direction with veering and backing winds in both hemispheres by means of large-eddy simulations. Likewise we quantify the sensitivity of the wake to the strength of stratification, the strength and type of wind veer, and the wind speed in the Northern Hemisphere. A veering wind in combination with counterclockwise rotating blades would result in a power output increase of 11.5% for a downwind turbine in comparison to a clockwise rotating upwind turbine in the Northern Hemisphere. In the Southern Hemisphere, the power output of a downwind turbine would decrease by the same value if the upwind turbine rotates counterclockwise. These wake differences result from the interaction of a veering or a backing wind with the rotational direction of the near wake. In the common case of a clockwise rotating rotor and a veering wind in the Northern Hemisphere, or similarly a backing wind in the Southern Hemisphere, the rotational direction differs in the far wake compared to the near wake. In contrast, if a counterclockwise rotating rotor interacts with a veering wind in the Northern Hemisphere or a backing wind in the Southern Hemisphere, the rotational direction of the near wake persists throughout the entire wake. Under veering wind conditions in the Northern Hemisphere, enhancing the thermal stability or increasing the strength of the veering wind further enlarges the power output difference up to 23%. The positive impact on the potential power production can be explained by an intensified entrainment of the ambient air and the more rapid wake recovery under shared wind conditions and counterclockwise rotating blades.

https://doi.org/10.5194/wes-2019-105
Preprint. Discussion started: 28 January 2020

eawe european academy of wind energy
Open Access WIND ENERGY SCIENCE DISCUSSIONS

1 Introduction

Most modern industrial-scale wind turbines rotate clockwise, as seen from a viewer looking downwind. Traditional Danish windmills turned counterclockwise due to the thin end of the laths pointing towards the left on the blades as they were built by right-handed millers. This rotational direction was adapted by the wind-turbine pioneer Christian Riisager and also by Tvind. In 1978, Erik Grove-Nielson designed the first 5 m fibreglass blades. He and his wife Tove decided for a clockwise rotational direction of the blades purportedly to distinguish their product from Tvind. Therefore, the first modern wind turbines rotated in both directions. Descendants of the Riisager wind turbine (Wind Matic and Tellus) rotate counterclockwise and of Grove-Nielson (Vestas, Bonus (now Siemens), Nordtank and Enercon) clockwise. Three of the four clockwise rotating blade manufacturers became market leaders in the international wind power industry, and the clockwise rotating blades, eventually, became the global standard (Maegaard et al., 2013). The clockwise blade rotation is, therefore, barely a historical coincidence without any physical motivation.

Rotating blades are faced by a variety of wind conditions. In a convective regime during daytime, there is no significant change of the incoming wind direction or wind speed with height and the inflow conditions are rather uniform over the whole rotor area. A nocturnal stably stratified regime, however, often generates wind profiles with changing magnitude (vertical wind shear) and direction (wind veer). Vertical variations of both quantities reflect the Coriolis force and friction. Friction affects the lowest part of the wind profile while the rotational direction of the wind vector in the Ekman spiral aloft depends on the hemisphere. In the Northern Hemisphere (NH) (Southern Hemisphere (SH)), winds tend to rotate clockwise (counterclockwise) with height (Stull, 1988). This veering wind is associated with warm air advection and dynamic lifting. It changes in cases of cold air advection or dynamic sinking into a backing wind, which is characterized by a counterclockwise (clockwise) wind direction change with height in the NH (SH). In addition, frontal passages or topographically-driven phenomena such as drainage flows may modify this typical background veer (Walter et al., 2009; Bodini et al., 2019; Sanchez Gomez and Lundquist, 2019).

The wind turbine's wake characteristics in a veering wind regime differ for counterclockwise and clockwise rotating blades as shown by Englberger et al. (2019). The rotational direction of the near wake is mainly determined by the rotation of the blades, whereas the rotational direction of the far wake is determined by the Ekman spiral. If a northern hemispheric Ekman spiral interacts with clockwise rotating blades, the near wake's counterclockwise rotation diminishes and becomes clockwise in the far wake. Conversely, if the same flow interacts with counterclockwise rotating blades, the near wake rotates in a clockwise direction. In contrast to the former case, the rotational direction persists in the whole wake, as the stably stratified regime in the NH results also in a clockwise flow rotation of the far wake. However, the rotational direction impact is rather small in a flow regime without significant vertical wind shear and no wind veer in the height of the rotor (Vermeer et al., 2003; Shen et al., 2007; Sanderse, 2009; Kumar et al., 2013; Hu et al., 2013; Yuan et al., 2014; Mühle et al., 2017; Englberger et al., 2019).

This interaction of the rotational direction of a wind turbine with a veering wind suggests that a preferential rotational direction of a wind turbine in a stably stratified atmospheric boundary layer (ABL) on each hemisphere could exist. The term

https://doi.org/10.5194/wes-2019-105
Preprint. Discussion started: 28 January 2020

eawe european academy of wind energy
Open Access WIND ENERGY SCIENCE DISCUSSIONS

'preferential' refers to the positive impact on a downwind turbine's inflow velocity (less perturbed and higher magnitude) and, therefore, its potentially larger power output.

We investigate the relationship between the upstream wind profile and the direction of the turbine rotation by large-eddy simulations (LESs). Both clockwise and counterclockwise rotating actuators are embedded in stably stratified atmospheric flows representing a veering as well as a backing wind for the NH and also for the SH. In addition, we investigate the impact of the rotational direction of the blades for different strengths of the stably stratified regime, for different amounts of wind direction changes with height, for different rotor parts affected by the veering wind, and also for different wind speeds. Altogether, 24 combinations of rotor rotation and inflow wind conditions in a stably stratified ABL are simulated.

To our knowledge, this is the first study which investigates the impact of the rotational direction in combination with an Ekman spiral on wake characteristics, which are relevant for the performance of a downwind turbine and for wind turbine control strategies (Fleming et al., 2019).

The previous study Englberger et al. (2019) lays the groundwork for this study, describing in detail the rotational direction impact in veered and non-veered situations (in the Northern Hemisphere). Further, it explains the physical mechanism responsible for the rotational direction impact of the blades on the wake by a simple linear superposition of the veering inflow wind field and a wind-turbine model, which includes a Rankine vortex.

This paper is organised as follows. The numerical model EULAG and the wind-turbine simulation setup are described in Sect. 2. The rotational direction impact on the wake follows in Sect. 3, investigating the difference of a veering wind and a backing wind on both hemispheres, the impact of the strength of stratification, the strength of the veering wind, the type of the veering wind, and the wind speed for a veering wind in the NH. A conclusion is given in Sect. 4.

2 Numerical Model Framework

2.1 The Numerical Model EULAG

The dry ABL flow through a wind turbine is simulated with the multiscale geophysical flow solver EULAG (Prusa et al., 2008). A comprehensive description and discussion of EULAG can be found in Smolarkiewicz and Margolin (1998) and Prusa et al. (2008).

The Boussinesq equations for a flow with constant density ρ_0 = 1.1 kg m^{-3} are solved for the Cartesian velocity components u, v, w and for the potential temperature perturbations $\Theta' = \Theta - \Theta_{BL}$ (Smolarkiewicz et al., 2007),

$$\frac{d\mathbf{v}}{dt} = -\boldsymbol{\nabla}\left(\frac{p'}{\rho_0}\right) + \mathbf{g}\frac{\Theta'}{\Theta_0} + \boldsymbol{\mathcal{V}} - 2\Omega\left(\mathbf{v} - \mathbf{v}_{BL}\right) + \boldsymbol{\beta}_{\mathbf{v}}\frac{\mathbf{F}_{WT}}{\rho_0}, \tag{1}$$

$$\frac{d\Theta'}{dt} = \mathcal{H} - \mathbf{v}\nabla\Theta_{BL}, \tag{2}$$

$$\boldsymbol{\nabla}\cdot(\rho_0\mathbf{v}) = 0, \tag{3}$$

https://doi.org/10.5194/wes-2019-105
Preprint. Discussion started: 28 January 2020

eawe european academy of wind energy
Open Access WIND ENERGY SCIENCE DISCUSSIONS

where Θ_0 represents the constant reference value of 300 K and u_{BL}, v_{BL}, w_{BL}, and Θ_{BL} are height dependent environmental states. In Eqs. (1), (2) and (3), d/dt, $\boldsymbol{\nabla}$ and $\boldsymbol{\nabla}\cdot$ represent the total derivative, the gradient and the divergence, respectively. The quantity $p^{'}$ represents the pressure perturbation with respect to the environmental state and $\mathbf{g}$ the vector of acceleration due to gravity. The subgrid-scale terms $\boldsymbol{\mathcal{V}}$ and $\mathcal{H}$ symbolise viscous dissipation of momentum and diffusion of heat and the Coriolis force is represented by the angular velocity vector of the earth's rotation. $\mathbf{F}_{WT}$ corresponds to the turbine-induced force, parametrized with the blade element momentum (BEM) method as rotating actuator disc with both rotational directions $\boldsymbol{\beta_v}$. All following simulations are performed with a TKE closure (Schmidt and Schumann, 1989; Margolin et al., 1999).

2.2 Setup of the Wind-Turbine Simulations

Wind-turbine simulations on 512 × 64 × 64 grid points with a horizontal and vertical resolution of 5 m and open horizontal boundaries are performed for a stably stratified ABL lasting 20 min. The rotor of the wind turbine has a diameter D as well as a hub height z_h of 100 m and is located at 300 m in x-direction and centred in the y-direction.

24 wind-turbine simulations explore the combinations of the incoming wind field and the rotational direction of the wind-turbine rotor. They are listed in Table 1. The simulations are initialized with the zonal velocity profile

$$u_{BL}(z) = u_g * \left(1 - exp\left(-\frac{z\sqrt{f/\kappa}}{\sqrt{2}}\right)\right), \tag{4}$$

with a geostrophic wind u_g, the Coriolis parameter $f = 1.0 \times 10^{-4}$ s^{-1}, and an eddy viscosity coefficient $\kappa = 0.06$ m^2 s^{-1}, following Shapiro and Fedorovich (2010). The corresponding meridional velocity profile is

$$v_{BL}(z) = u_{BL}(z) * tan(\phi_{wind}(z)) \tag{5}$$

with

$$\phi_{wind}(z) = \pm 2\Delta\phi\left(1 - \frac{z}{D}\right) \tag{6}$$

in the lowest 200 m and constant above.

In the incoming wind conditions we consider on the NH ($f > 0$) and the SH ($f < 0$) a veering ($\frac{\partial\phi_{wind}}{\partial z} < 0$ in NH, $\frac{\partial\phi_{wind}}{\partial z} > 0$ in SH) and a backing ($\frac{\partial\phi_{wind}}{\partial z} > 0$ in NH, $\frac{\partial\phi_{wind}}{\partial z} < 0$ in SH) wind. In the reference simulation with a veering wind on the NH, the wind direction change over the rotor radius is $\Delta\phi = 4°$ with $v_{BL}(z_h) = 0$. The vertical velocity is

$$w_{BL}(z) = 0 \tag{7}$$

in all simulations.

For a veering wind in the NH, we further modify the strength of $\Delta\phi$ over the rotor with 2°, 4°, and 8° corresponding to a weak (w), moderate (m), or strong (s) veer. We also test the rotational direction sensitivity towards the rotor section interacting with $\Delta\phi \neq 0$, limited to the lower rotor part (l) or extended over the entire rotor (e) and the geostrophic wind u_g with 10 m s^{-1} and 14 m s^{-1}.

https://doi.org/10.5194/wes-2019-105
Preprint. Discussion started: 28 January 2020

eawe european academy of wind energy
Open Access WIND ENERGY SCIENCE DISCUSSIONS

The potential temperature in the reference simulation is

$$\Theta_{BL}(z) = \Theta_0 + \frac{3\,K}{200\,m} z \tag{8}$$

in the lowest 200 m and 303 K above. We test the rotational direction sensitivity towards the strength of the stably stratified ABL and preformed simulations with 1.5 K / 200 m and 6 K / 200 m corresponding to weakly ($th15$) and strongly ($th60$) stably stratified regimes in addition to the moderate regime ($th30$) of the reference simulation.

We consider two different rotational directions of the rotor blades. As the forces $\mathbf{F}_{WT}$ acting on the velocity components in Eq. 1 simulate the air flow of the wake, a clockwise wake rotation is defined by β_v = -1 and β_w = 1 and a counterclockwise wake rotation by β_v = 1 and β_w = -1, with β_u = 1 in each simulation. A clockwise wake rotation is initiated by a counterclockwise blade rotation, due to conservation of angular momentum (e.g. described in Zhang et al. (2012)) and can be linked directly towards the opposite rotation of the rotor. Therefore, our simulations represent a clockwise rotor rotation CR and a counterclockwise rotor rotation CCR. Simulations with a clockwise rotating rotor CR corresponding to a counterclockwise rotating near wake are comparable to the CCW simulations in Englberger et al. (2019), and simulations with a counterclockwise rotating rotor CCR corresponding to a clockwise rotating near wake are comparable to CW (Englberger et al., 2019).

The turbine-induced forces $\mathbf{F}_{WT}$ are calculated with the BEM-method, including a nacelle at the center grid point and excluding the tower. For the airfoil data, the 10 MW reference wind turbine from DTU (Bak et al., 2013) is applied, whereas the radius of the rotor as well as the chord length of the blades are scaled down to the rotor with a diameter of 100 m. The rotation frequency is set to 7 rpm. A detailed description of the wind-turbine parametrization and the applied smearing of the forces, as well as all values used in the blade parametrization are given in Englberger and Dörnbrack (2017, parametrization B). A turbulent stably stratified regime in our wind-turbine simulations performed with open horizontal boundary conditions is verified by applying the parametrization of Englberger and Dörnbrack (2018b). All parameters required to apply the parametrization are described in detail in Englberger and Dörnbrack (2018b). A rather similar set-up, including the wind-turbine parametrization and the parametrization of the turbulent stably stratified regime, have been applied and explained in more detail in Englberger et al. (2019) and Englberger and Lundquist (2019).

3 Rotational Direction Impact on the Wake

In the following, the impact of the rotational direction of the rotor towards different atmospheric conditions is systematically investigated. Here, we consider the 10-min time and rotor area averaged streamwise velocity $\overline{u_A}$. It is further used to calculate the power produced by a hypothetical downwind turbine up to 10 D downstream with

$$P = \frac{1}{2}\,\rho_0\,c_p\,\eta_{mech}\,A\,\overline{u_A} \tag{9}$$

where ρ_0 is the density of the air, c_p = 0.5, η_{mech} = 0.64 and A the area of the rotor (Manwell et al., 2002). In the following, $\overline{u_A}$ and P are evaluated and discussed at all downwind positions from 4 D to 10 D, with special emphasis at 7 D, as a typical downwind distance for a hypothetical waked wind turbine (e.g. Gaumond et al. (2014); Abkar et al. (2016)). Further, we use

https://doi.org/10.5194/wes-2019-105
Preprint. Discussion started: 28 January 2020

eawe european academy of wind energy
Open Access WIND ENERGY SCIENCE DISCUSSIONS

Table 1. List of all performed simulations in this study for a clockwise and a counterclockwise rotor rotation. Here, b represents a backing wind and v a veering wind. $th15$ a low stably stratified regime and $th60$ a strongly stably stratified one. e and l correspond to the rotor position, which is affected by wind veer (entire (e) rotor or lower (l) rotor half). s and w corresponds to a strong or a weak wind veer and u14 to a higher geostrophic wind speed of 14 m s^{-1}. ϕ_{wind} results from Eq. 6. The simulations CR and CCR correspond to both reference simulations with opposite rotational direction with $CR\_v\_NH\_th30\_em\_u10$ and $CCR\_v\_NH\_th30\_em\_u10$. All _ to CR and CCR correspond to the differences between the corresponding simulation and its reference simulations CR and CCR.

SIMULATIONS WITH DIFFERENT ROTATIONAL DIRECTIONS OF THE ROTOR						
CLOCKWISE	ϕ_{wind}(150 m)	ϕ_{wind}(50 m)	$\frac{\partial\Theta}{\partial z}$	u$_g$	f	**COUNTERCLOCKWISE**
CR	-4°	4°	3 K / 200 m	10 m s^{-1}	>0	**CCR**
CR_b	4°	-4°	3 K / 200 m	10 m s^{-1}	>0	**CCR_b**
CR_v_SH	4°	-4°	3 K / 200 m	10 m s^{-1}	<0	**CCR_v_SH**
CR_SH	-4°	4°	3 K / 200 m	10 m s^{-1}	<0	**CCR_SH**
CR_th15	-4°	4°	1.5 K / 200 m	10 m s^{-1}	>0	**CCR_th15**
CR_th60	-4°	4°	6 K / 200 m	10 m s^{-1}	>0	**CCR_th60**
CR_es	-8°	8°	3 K / 200 m	10 m s^{-1}	>0	**CCR_es**
CR_ew	-2°	2°	3 K / 200 m	10 m s^{-1}	>0	**CCR_ew**
CR_ls	-8°	0°	3 K / 200 m	10 m s^{-1}	>0	**CCR_ls**
CR_lm	-4°	0°	3 K / 200 m	10 m s^{-1}	>0	**CCR_lm**
CR_u14	-4°	4°	3 K / 200 m	14 m s^{-1}	>0	**CCR_u14**
CR_es_u14	-8°	8°	3 K / 200 m	14 m s^{-1}	>0	**CCR_es_u14**

the velocity deficit, defined according to

$$VD_{i,j,k} = \frac{\overline{u_{i_1,j,k}} - \overline{u_{i,j,k}}}{\overline{u_{i_1,j,k}}}, \tag{10}$$

calculated at the discrete grid points x_i, y_j, and z_k with i_1 corresponding to the first upstream grid point.

3.1 Veering Wind vs. Backing Wind on both Hemispheres

The comparison of simulations CR and CR_b reveals the difference in $\overline{u_A}$ and P between a veering and a backing wind on the NH in case of a clockwise rotating rotor. Fig. 1a shows larger $\overline{u_A}$-values if a backing wind (CR_b) interacts with a clockwise rotating rotor in comparison to a veering wind (CR). In addition, the difference of $\overline{u_A}$ between a backing and a veering wind increases downwind up to $\Delta\overline{u_A} \approx 0.5$ m s^{-1} at 10 D. Considering a counterclockwise rotating rotor in CCR and CCR_b, $\Delta\overline{u_A}$ is the same for CR and CCR_b and likewise for CCR and CR_b. This results in larger $\overline{u_A}$-values and P-values in CCR in comparison to CCR_b. For a hypothetical 7 D downwind turbine, this leads to an 11.5% increase in power in case of a veering wind interacting with counterclockwise rotating blades or if a backing wind interacts with clockwise rotating blades.

https://doi.org/10.5194/wes-2019-105
Preprint. Discussion started: 28 January 2020

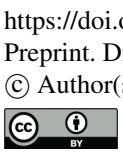

eawe european academy of wind energy
Open Access WIND ENERGY SCIENCE DISCUSSIONS

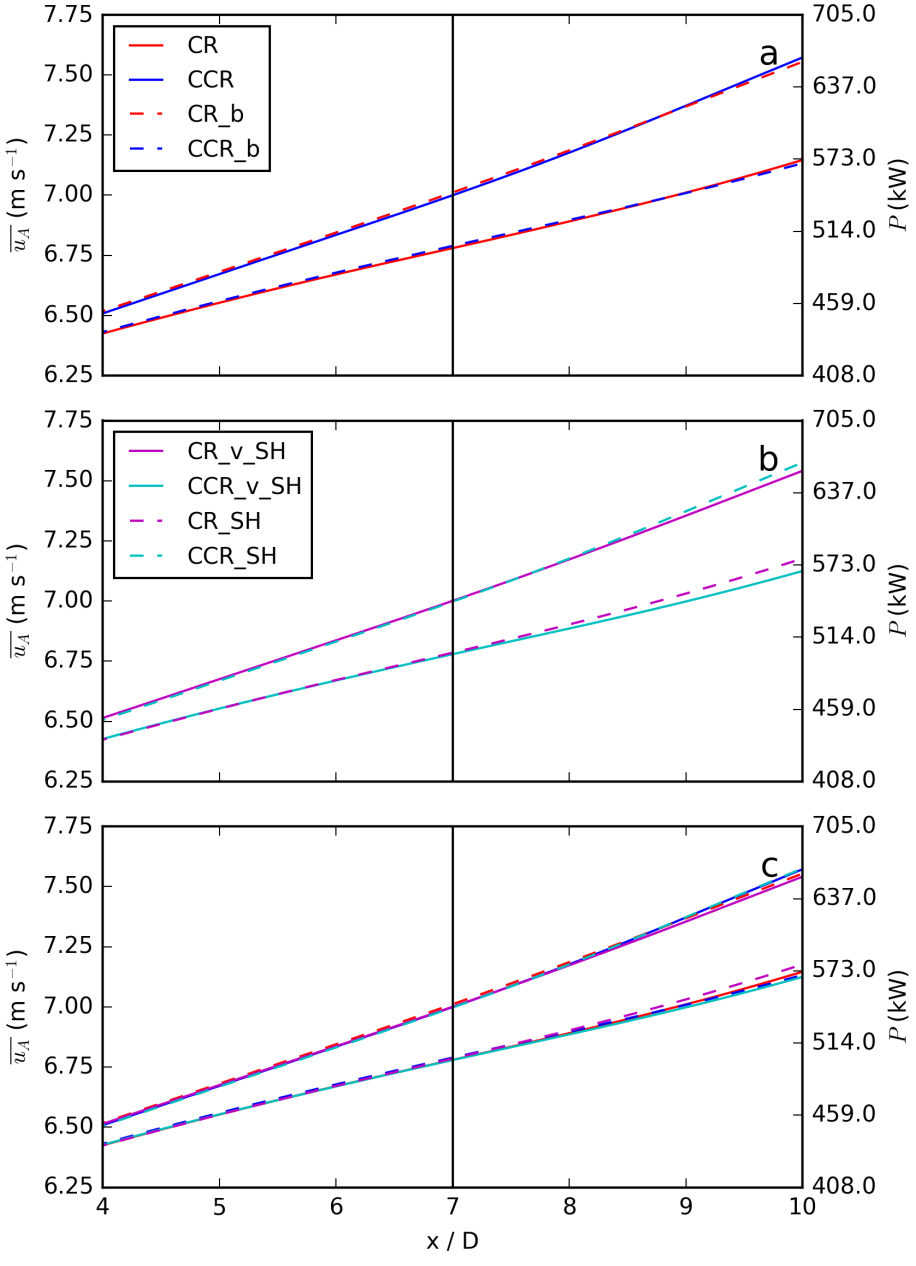

Figure 1. The rotor averaged streamwise velocity $\overline{u_A}$ and the power P of a hypothetical downwind turbine are presented for a downstream region of $[4\,D; 10\,D]$ for a veering and a backing wind in the NH in a, for a veering and a backing wind in the SH in b, and for all eight simulations together in c.

https://doi.org/10.5194/wes-2019-105
Preprint. Discussion started: 28 January 2020

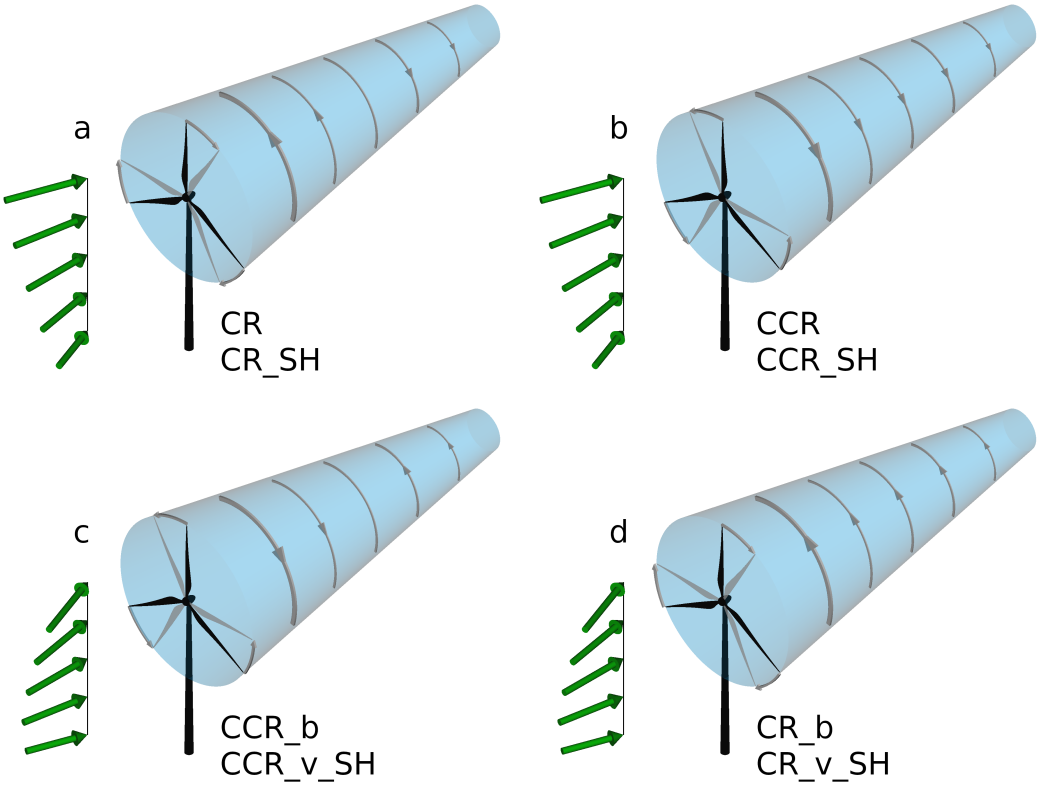

Figure 2. Schematic illustration of the rotational direction of the wake for the cases: Clockwise blade rotation with veering wind in NH (CR) and with backing wind in SH (CR_SH) in (a), counterclockwise blade rotation with veering wind in NH (CCR) and backing wind in SH (CCR_SH) in (b), counterclockwise blade rotation with backing wind in NH (CCR_b) and veering wind in SH (CCR_v_SH) in (c), and clockwise blade rotation with backing wind in NH (CR_b) and veering wind in SH (CR_v_SH) in (d).

The same investigation is shown in Fig. 1b for the SH. Here, we also consider a veering and a backing wind with both rotational directions of the rotor, resulting in the simulations CR_v_SH, CCR_v_SH, CR_SH, and CCR_SH. The downstream behaviour and likewise $\Delta\overline{u_A}$ are similar but opposite to the results in the NH. The power output of a hypothetical downwind turbine at 7 D would also be larger by 11.5%, however, on the SH, in case of a veering wind and clockwise rotating blades or a backing wind interacting with counterclockwise rotating blades. The minor difference near 10 D downwind between CR_v_SH and CCR_SH and likewise between CCR_v_SH and CR_SH in Fig. 1b results from the applied parametrization of Englberger and Dörnbrack (2018b), as the inflow wind field was extracted from a diurnal cycle LES on the NH (Englberger and Dörnbrack, 2018a). This assumption is supported by the following aspects: the difference is not prevalent in the northern hemispheric simulations in Fig. 1a, and the difference emerges far downstream, starting at $x > 8$ D, where the impact of the disc on the wake structure is rather small in comparison to the ambient flow field impact and it also increases approaching 10 D.

https://doi.org/10.5194/wes-2019-105
Preprint. Discussion started: 28 January 2020

eawe european academy of wind energy
Open Access WIND ENERGY SCIENCE DISCUSSIONS

In Fig. 1c, all eight simulations are shown. Here, the results of simulations CCR, CR_b, CR_v_SH, and CCR_SH overlap and, likewise, the ones for CR, CCR_b, CCR_v_SH, and CR_SH. The resulting flow fields of the wakes are schematically shown in Fig. 2. The combinations of $\frac{\partial \phi_{wind}}{\partial z} < 0$ and a clockwise blade rotation (Fig. 2a) or $\frac{\partial \phi_{wind}}{\partial z} > 0$ and a counterclockwise blade rotation (Fig. 2c) result in contrasting rotational directions of the near and far wake, referred to hereafter as 'contrasting wake cases'. The combinations of $\frac{\partial \phi_{wind}}{\partial z} < 0$ and a counterclockwise blade rotation (Fig. 2b) or $\frac{\partial \phi_{wind}}{\partial z} > 0$ and a clockwise blade rotation (Fig. 2d), however, result in a rotational direction of the wake which persists in the whole wake, referred to hereafter as 'consistent wake cases'. This contrasting and consistent behaviour of the rotational direction in the wake is valid on both hemispheres.

The 10-min time averaged streamwise velocity, representing the simulation from 10 min to 20 min, is plotted at hub height in Fig. 3 for all eight cases together with the velocity deficit (Eq. 10) as contour. The structures of the four contrasting wake cases (left row) resemble each other with narrower wakes. Similarly, the four consistent wake cases (right row) resemble each other with wider wakes. The entrainment of ambient air in the consistent wake cases is slightly less rapid in the near wake in comparison to the contrasting wake cases, whereas it is substantially enhanced in the far wake. This results in the higher $\overline{u_A}$-value in the consistent wake cases and an increase of $\Delta\overline{u_A}$ approaching downstream with rather similar values in the near wake for $x < 4\,\mathrm{D}$ (Fig. 1). The wake structure dependence on the rotational direction of the rotor concurs with the results in Fig. 4 of Englberger et al. (2019).

The evolving different wake structures result in a larger power output of the consistent wake cases in comparison to the contrasting wake cases of a downwind turbine of roughly 11% at 7 D approaching even to 19% at 10 D. Considering the much higher frequency of occurrence of a veering wind in comparison to a backing wind (≈3.8 times more frequent according to two years of meteorological tower measurements in Lubbock (Texas) (Walter et al., 2009)), a counterclockwise rotating rotor in the NH (and a clockwise rotating rotor in the SH) would increase the power production for a waked turbine downwind.

3.2 Strength of Stratification

The impact of the stable stratification is tested for three different regimes, a weakly stably stratified atmosphere in CR_th15, a moderate stably stratified atmosphere in CR, and a strongly stably stratified atmosphere in CR_th60. The tested lapse rates are representative compared to Fig. 2 in Walter et al. (2009). The impact on $\overline{u_A}$ is presented in Fig. 4a. In case of a common clockwise rotating rotor, the wake lasts longer in stronger stratification in Fig. 4. The wake recovers faster in CR_th15 compared to CR and further CR recovers faster compared to CR_th60. This differences in $\overline{u_A}$ translates in a 19% larger power output of a hypothetical downwind turbine in an ABL during the evening transition (CR_th15) in comparison to the power output at night where the surface fluxes are at its minimum (CR_th60). Following the increase of the recovery rate from CR_th60 to CR to CR_th15, it would result in an increase of the power output for decreasing the strength of stratification.

Considering the same stratification with a counterclockwise rotating rotor in CCR_th15, CCR, and CCR_th60 in Fig. 4a, the values of downwind wind speed $\overline{u_A}$ are rather similar and nearly independent of the stratification. Only in the strongly stratified regime CCR_th60, the $\overline{u_A}$-value slightly increases in comparison to the weakly (4%) and moderate (3%) regimes,

https://doi.org/10.5194/wes-2019-105
Preprint. Discussion started: 28 January 2020

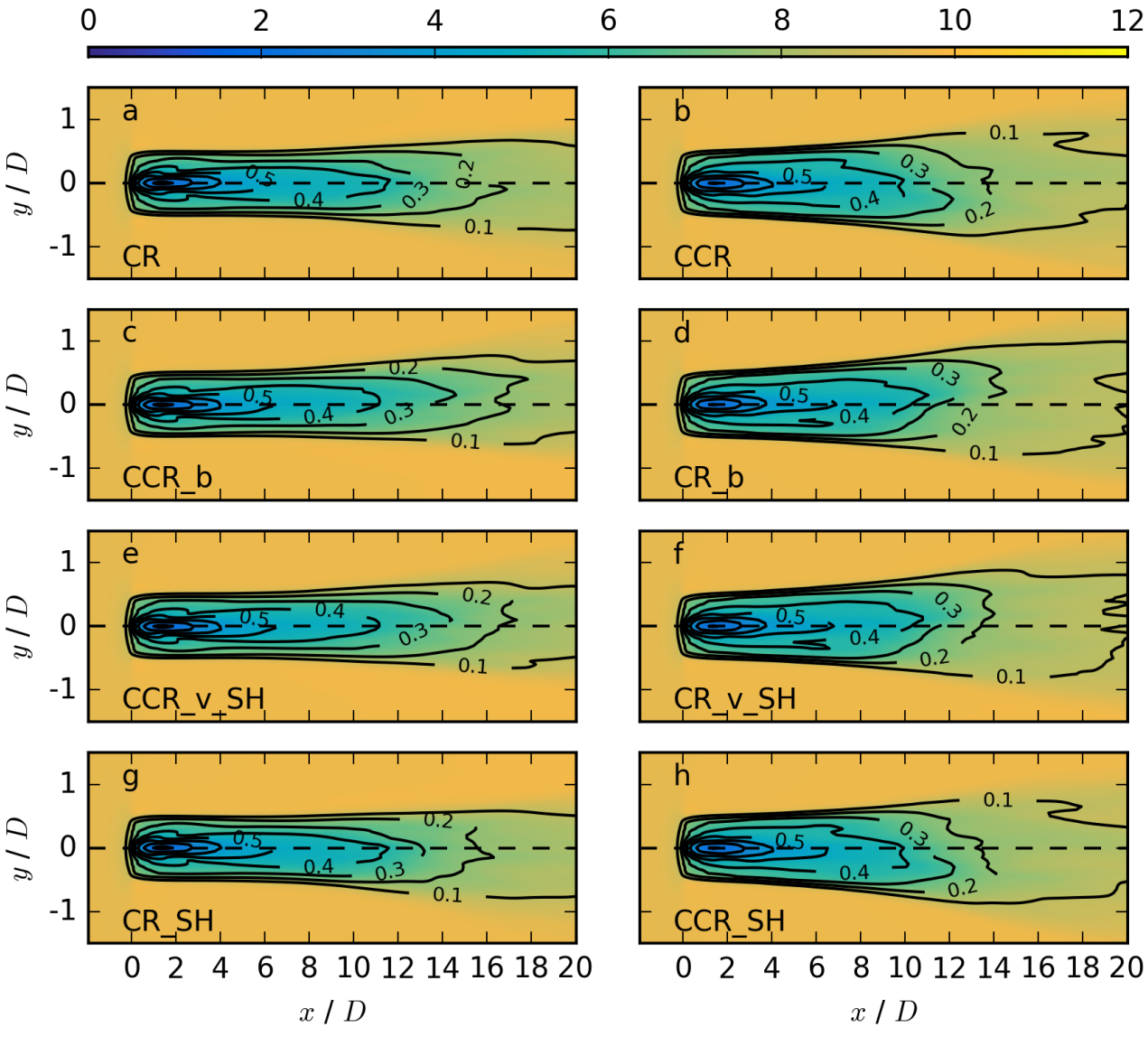

Figure 3. Coloured contours of the streamwise velocity $\overline{u_{i,j,k_h}}$ in m s^{-1} at hub height k_h, averaged over the last 10 min, for CR in (a), CCR in (b), CCR_b in (c), CR_b in (d), CCR_v_SH in (e), CR_v_SH in (f), CR_SH in (g), and CCR_SH in (h). The black contours represent the velocity deficit VD_{i,j,k_h} at the same vertical location.

https://doi.org/10.5194/wes-2019-105
Preprint. Discussion started: 28 January 2020

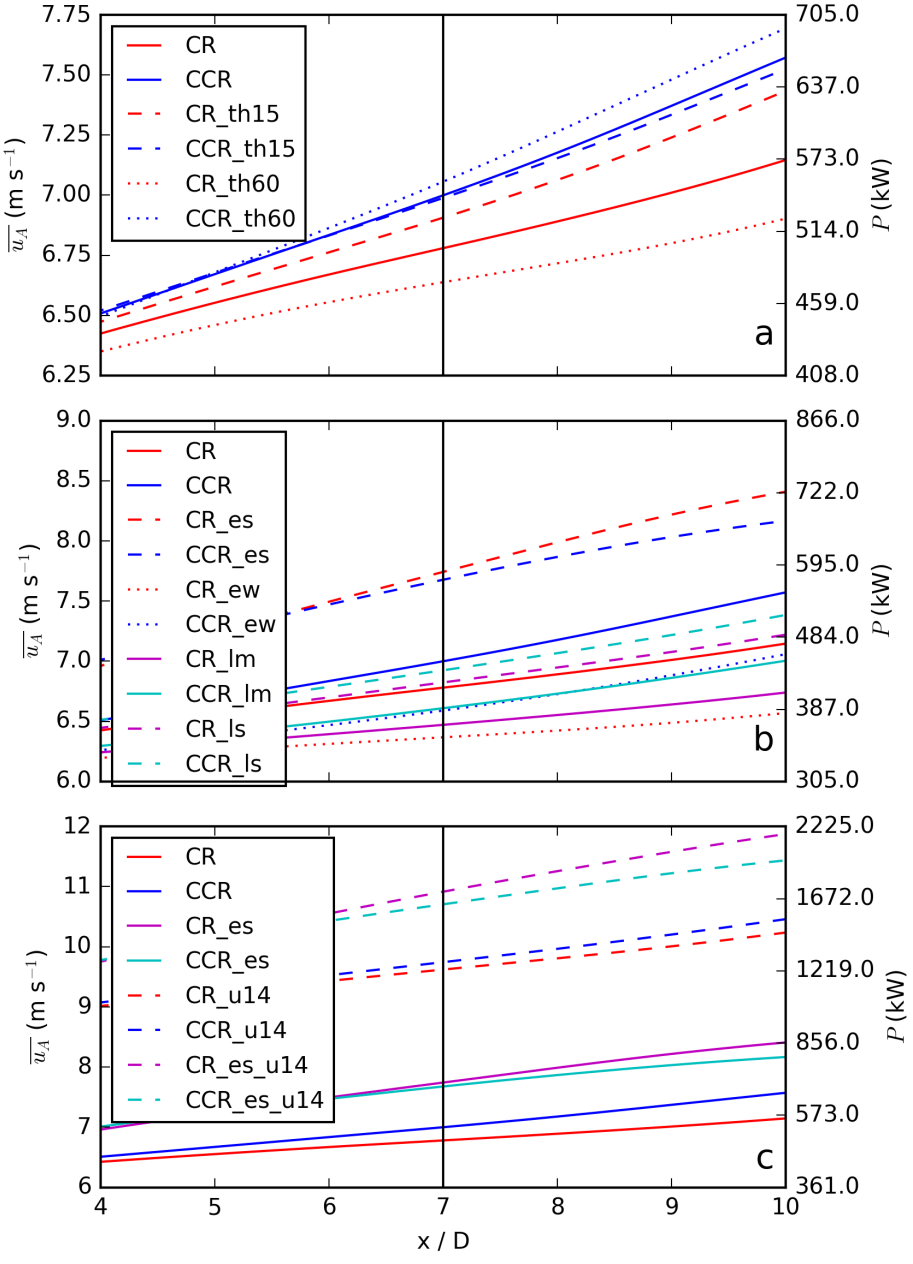

Figure 4. The rotor averaged streamwise velocity $\overline{u_A}$ and the power P of a hypothetical downwind turbine are presented for a downstream region of $[4\,D; 10\,D]$ for different thermal stratifications in a, for different strength of wind veer and rotor areas affected by the veering wind in b, and for different wind speeds in c.

https://doi.org/10.5194/wes-2019-105
Preprint. Discussion started: 28 January 2020

resulting in a maximum power output of a hypothetical downwind turbine at night where the surface fluxes approaching its minimum. However, the impact of stratification is roughly five times smaller in comparison to the one for clockwise rotating wind turbines.

This wake behaviour results in a larger potential power output of a downwind turbine in case of a counterclockwise rotating rotor of 4% in the weakly stably stratified case, of 11.5% in the moderate stably stratified case, and of 23% in the strongly stably stratified situation at 7 D. A counterclockwise blade rotation will not only enhance the power output, it will further increase the accumulated power output during the rather long nights with approximately constant surface fluxes (9 h (Walter et al., 2009, Fig. 2), 11 h (Blay-Carreras et al., 2014; Abkar et al., 2016; Englberger and Dörnbrack, 2018a, Fig. 1)). In addition, counterclockwise blade rotation would also increase the power output during the morning boundary layer regime. This ABL regime is strongly affected by the previous nocturnal stability with an even smaller entrainment rate before the surface fluxes become positive due to the incoming solar radiation (Englberger and Dörnbrack, 2018a, Fig. 4).

The contrasting power production between the clockwise and the counterclockwise rotating simulations can be explained by means of Fig. 5. The wake structure in the clockwise rotating blade simulations CR_th15 in a, CR in c, and CR_th60 in e, behaves as known from previous studies: a less rapid wake recovery and an elongated wake for a stronger stably stratified regime (Abkar and Porté-Agel, 2014; Abkar et al., 2016; Vollmer et al., 2016; Englberger and Dörnbrack, 2018a). In contrast, the wake structures are rather similar in CCR_th15 in b and in CCR in d. Only the wake width of CCR_th60 in f differs slightly from CCR_th15 and CCR. A significant difference in the wake elongation, as in the CR simulations, however, can not be detected in the CCR simulations. This significant difference in the entrainment process results from the different behaviour in the wake rotation approaching downstream between the contrasting wake cases CR and the consistent wake cases CCR (Fig. 2) and is responsible for an increase of a downwind turbines power output up to 23% for counterclockwise rotating blades instead of clockwise ones.

3.3 Strength of Veering Wind

The impact of the strength of wind veer over the rotor is investigated for $\Delta\phi$-values of 2°, 4°, and 8°, corresponding to a weak (w), moderate (m), or strong (s) change in CR_es, CR, and CR_ew and plotted in Fig. 4b. If the strength of veer increases, the corresponding $\overline{u_A}$-value increases. Again, this effect is related to a more rapid entrainment of ambient air into the wake. Considering a counterclockwise rotating rotor, the power output in the weak case would be 13% larger at 7 D in comparison to a clockwise rotating one. In the moderate case it would increase by 11%. In the strong case, however, it would slightly decrease by 3%. According to Fig. 3 in Walter et al. (2009), a veering wind of 2° has the highest measured occurring frequency of 9% and a veering wind of 4° has a frequency of 6%. A veering wind of 8°, which would slightly decrease the power output for changing the rotational direction of the rotor, however, occurs only 3% of the time. The probability of occurrence for an even higher wind veer corresponding to a higher power output for a clockwise rotating rotor in comparison to a counterclockwise rotating one decreases up to 1% for $\Delta\phi = 14°$.

The difference in the power values between the clockwise and the counterclockwise rotating simulations in the strong, moderate, and weak veer cases can be explained by means of Fig. 6. In the clockwise rotating blade simulations CR_ew in a,

https://doi.org/10.5194/wes-2019-105
Preprint. Discussion started: 28 January 2020

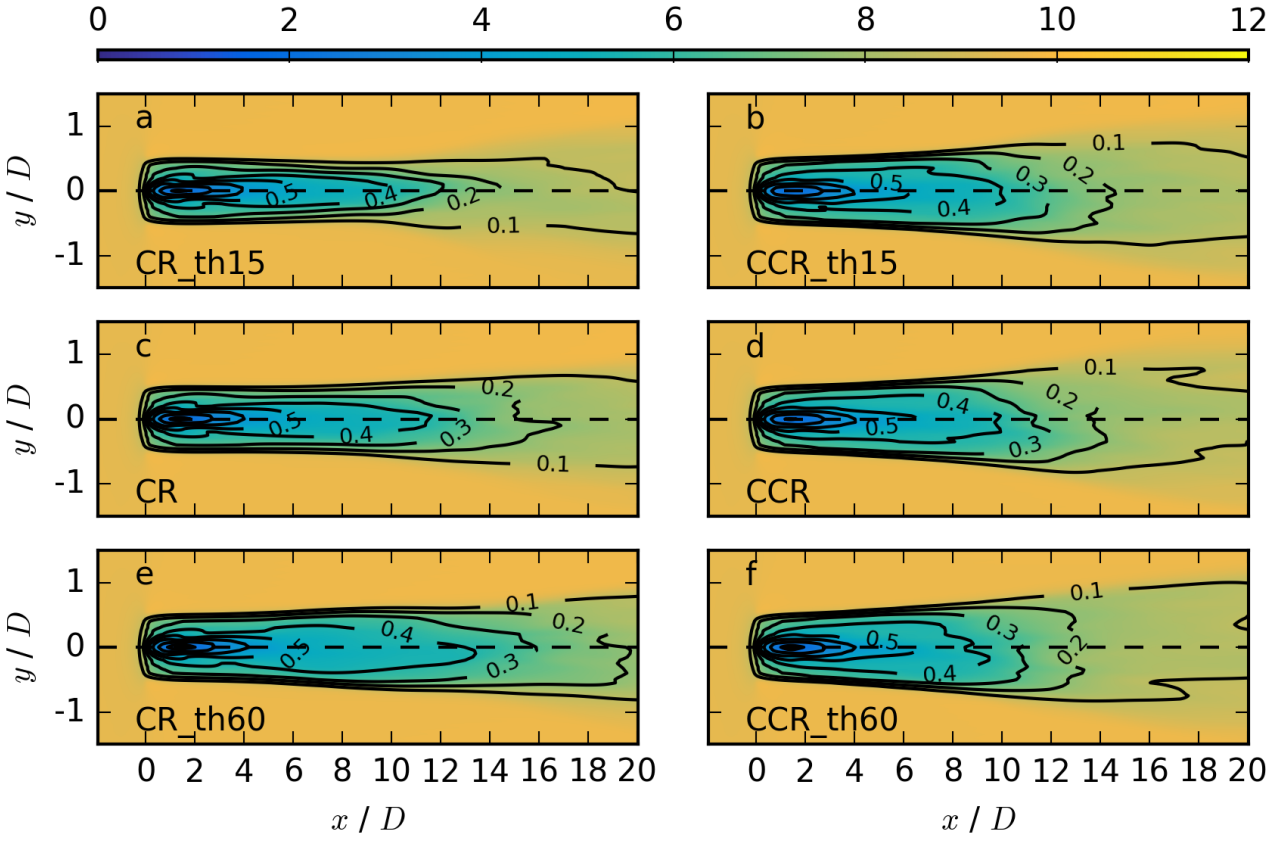

Figure 5. Coloured contours of the streamwise velocity $\overline{u_{i,j,k_h}}$ in m s^{-1} at hub height k_h, averaged over the last 10 min, for CR_th15 in (a), CCR_th15 in (b), CR in (c), CCR in (d), CR_th60 in (e), and CCR_th60 in (f). The black contours represent the velocity deficit VD_{i,j,k_h} at the same vertical location.

CR in c, and CR_es in e, the wake recovers more rapidly if the strength of wind veer increases, due to amplified turbulence production and, therefore, higher entrainment rates. Our simulated dependence of the wake recovery on the amount of wind veer is comparable to the results in Fig. 11 of Bhaganagar and Debnath (2014). Considering the corresponding counterclockwise rotating blade simulations CCR_ew in b, CCR in c, and CCR_es in e, the amount of wind veer affects the wake elongation, however, the difference between strong, moderate, and weak wind veer is much smaller in comparison to the corresponding CR simulations. In detail, the wake elongation in CR_ew is much longer in comparison to CCR_ew. It is still larger in CR in comparison to CCR. These differences between the CR and the CCR simulations result in the larger power output of 13% in the strong veer CCR cases and of 11% in the moderate veer CCR cases. Further, the difference between CR_ew and CR is larger in comparison to CCR_ew and CCR. Both wake elongation trends continue for an increasing amount of veer. It finally

https://doi.org/10.5194/wes-2019-105
Preprint. Discussion started: 28 January 2020

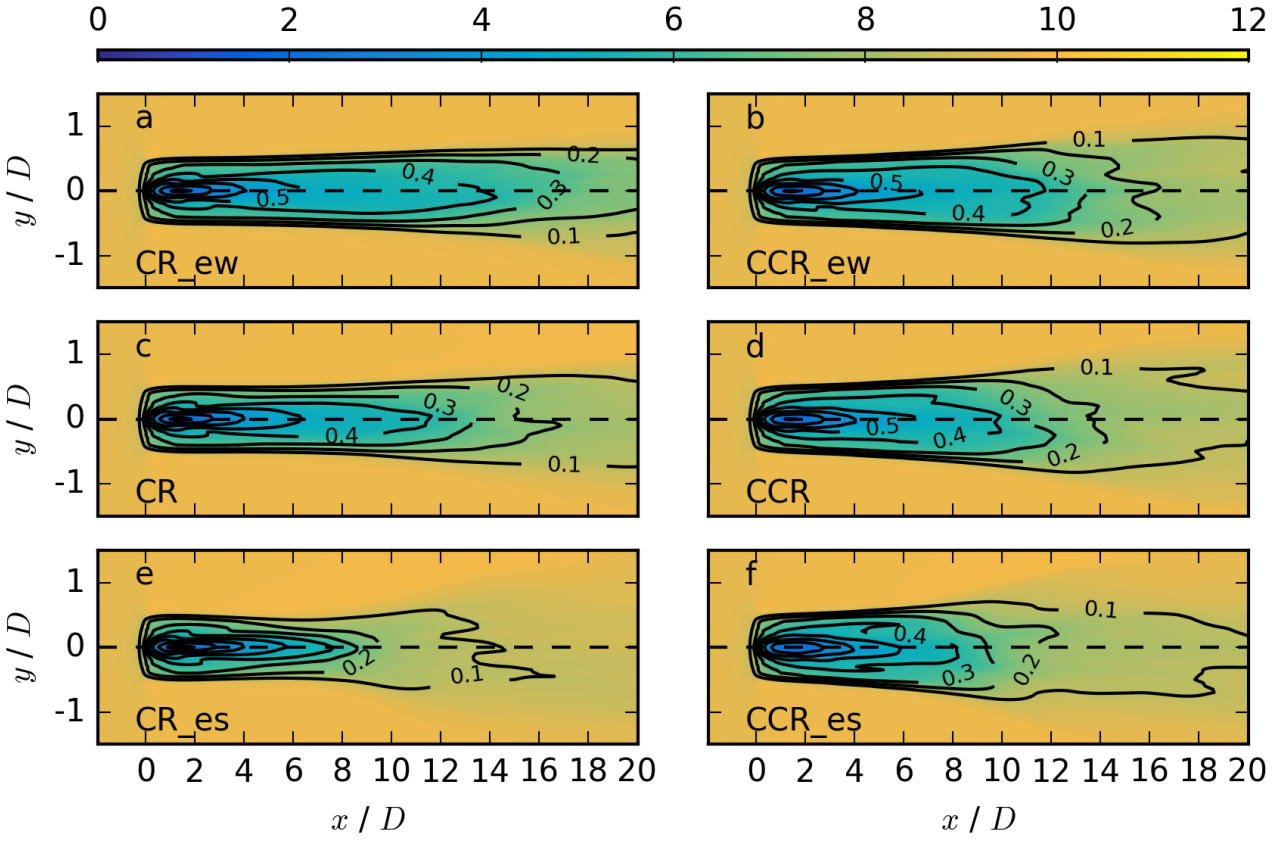

Figure 6. Coloured contours of the streamwise velocity $\overline{u_{i,j,k_h}}$ in m s^{-1} at hub height k_h, averaged over the last 10 min, for CR_ew in (a), CCR_ew in (b), CR in (c), CCR in (d), CR_es in (e), and CCR_es in (f). The black contours represent the velocity deficit VD_{i,j,k_h} at the same vertical location.

results in a faster wake recovery of CR_es in comparison to CCR_es, which is responsible for the slightly larger power output of CR_es in comparison to CCR_es.

3.4 Type of Veering Wind

The impact of the rotor section (entire rotor e, lower rotor half l) interacting with a veering wind is investigated by comparing CR to CR_lm and CR_es to CR_ls in Fig. 4*b*. Due to less mixing, the $\overline{u_A}$-value is much smaller in CR_lm in comparison to CR (16%) and likewise in CR_ls in comparison to CR_es (49%). Considering CCR_lm, the rotational direction impact on $\overline{u_A}$ is rather similar as in the corresponding full wake CCR simulations (7% vs. 11%). Further, considering CCR_ls, $\overline{u_A}$ increases in comparison to CCR_lm due to a higher entrainment rate. However, compared to CR_es and CCR_es, here the $\overline{u_A}$-value is still larger in case of a counterclockwise rotating rotor, resulting in an additional power gain of 4% for a

https://doi.org/10.5194/wes-2019-105
Preprint. Discussion started: 28 January 2020

eawe european academy of wind energy
Open Access WIND ENERGY SCIENCE DISCUSSIONS

counterclockwise rotating rotor instead of a clockwise rotating one. This is related to less turbulent mixing as the veering wind is only limited to the lower rotor half in CR_ls in comparison to the entire rotor in CR_es.

3.5 Wind Speed

The impact of the wind speed is investigated in Fig. 4*c*. Here, the geostrophic wind is increased from 10 m s^{-1} to 14 m s^{-1} in the simulations CR_u14 and CR_es_u14 for both rotational directions. Increasing the wind speed results in a larger entrainment rate and, therefore, in larger $\overline{u_A}$-values at the same downstream position. In case of moderate veer, the power output is 11% larger for counterclockwise rotating blades and u_g = 10 m s^{-1} and 4% for u_g = 14 m s^{-1}. In case of strong veer, however, the power output of the combination of u_g = 10 m s^{-1} and CR decreases the power output by 3% and the combination with u_g = 14 m s^{-1} by 7%. Therefore, an increase of wind speed does not clearly impact the power output difference. The behaviour is determined by the strength of the veering wind with an increase in the strong veer case and a decrease in the moderate veer case.

3.6 Summary

The relation between clockwise and counterclockwise rotating blades is shown in Fig. 7 for a downstream distance of 7 D. The 'ref' case presents the relation between CR and CCR. P(CR_α) / P(CR) - 1 is plotted on the x-axis and P(CCR_α) / P(CR) - 1 on the y-axis. As the value is above the black 1:1 line, the 'ref' case results in a larger power output of a downwind turbine at 7 D if the upwind turbine rotates counterclockwise, as shown in Fig. 1. In 'ref', the power output in case of CCR in comparison to CR is 11.5% larger. This is the vertical difference of 'ref' from the 1:1 line. The point 'b' represents the relation between P(CR_b) / P(CR) - 1 on the x-axis and P(CCR_b) / P(CR) - 1 on the y-axis. Here, P(CR_b) < P(CCR_b) with Δ P = -11.5% (distance from 'b' to 1:1 line). The points representing the cases CR_v_SH and CR_SH are almost identical with CR_b and CR and therefore with 'b' and 'ref'.

The point 'th15' represents a power increase by 4% at 7 D for CCR_th15 in comparison to CR_th15. Further, in comparison to 'ref', the power output of a downwind turbine in case of CR_th15 would be larger than for CR with a difference of 7% (Δ P on x-axis). Likewise, the power output of a downwind turbine in case of CCR_th15 would be slightly smaller than for CCR with a difference of 1% (Δ P on y-axis). Considering 'th60', a counterclockwise rotating rotor results in a 23% higher power output for a hypothetical downwind turbine placed at 7 D. Compared to 'ref' (and 'th15'), the power difference in case of a clockwise blade rotation is Δ P = - 7% (- 14%) and in case of a counterclockwise blade rotation Δ P = 3% (4%).

The same investigation is presented in Fig. 7 for CR_es vs. CCR_es in 'es', CR_ew vs. CCR_ew in 'ew', CR_ls vs. CCR_ls in 'ls', and CR_lm vs. CCR_lm in 'lm' and CR_u14 vs. CCR_u14 and CR_es_u14 vs. CCR_es_u14.

In Fig. 7, squared markers represent cases of strong entrainment processes in the wake of the upwind turbine e.g. 'th15' weak stably stratified regime, 'es' strong wind veer over the whole rotor, 'ls' strong wind veer limited to the lower rotor part. Circles represent moderate forcings and entrainment processes like 'ref'($th30$ moderate stably stratified regime and em moderate wind veer over the entire rotor) and triangles represent weak entrainment processes in the wake e.g. 'th60' strong stably stratified regime, 'ew' weak wind veer over the whole rotor. The differences in the entrainment rate can be seen in Figs. 5 and 6. From

https://doi.org/10.5194/wes-2019-105
Preprint. Discussion started: 28 January 2020

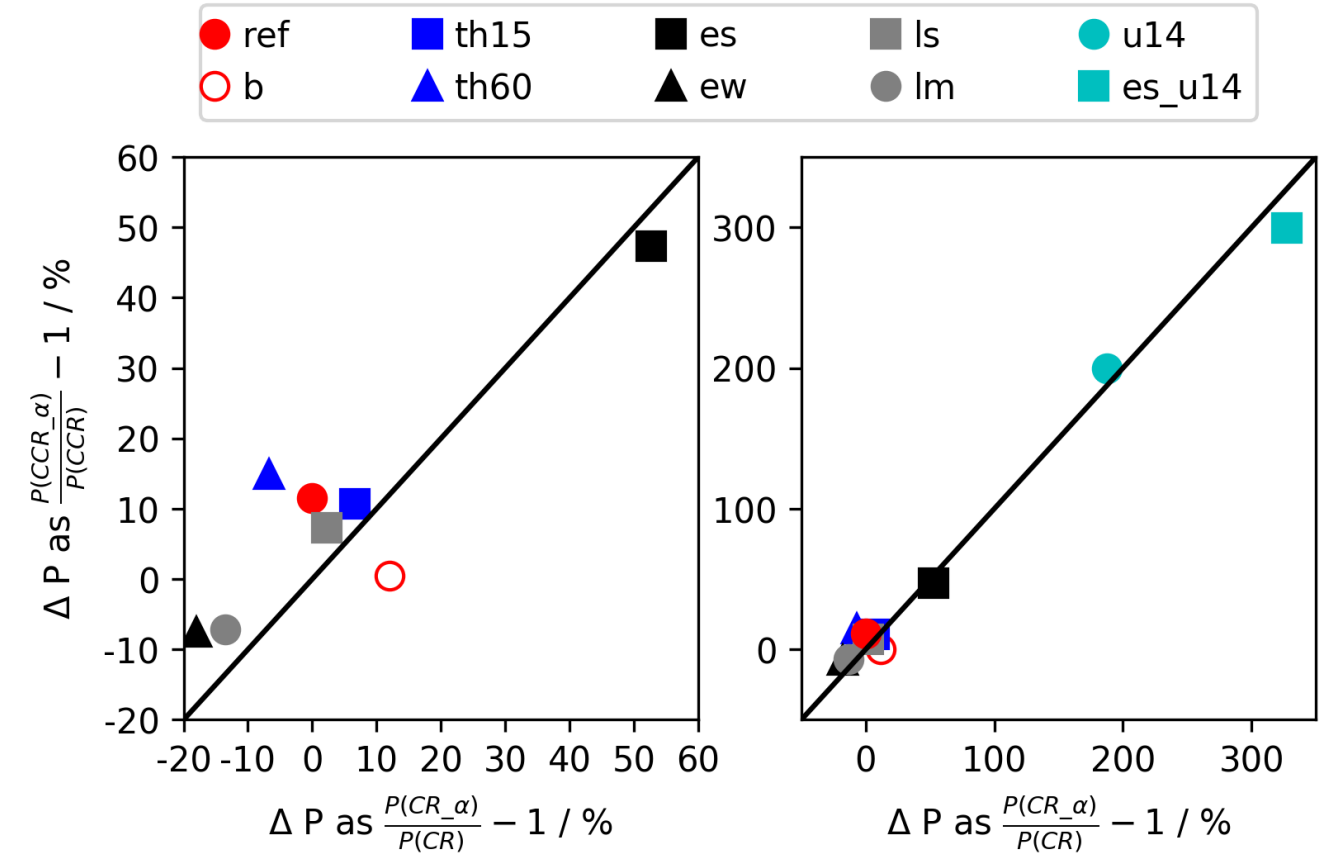

Figure 7. Power output difference of a hypothetical downwind turbine at a downstream distance of 7 D, if the upwind turbine rotates counterclockwise instead of the common clockwise blade rotation (deviation from 1:1 line) and likewise the power difference for the CR and the CCR simulations α in comparison to ref (x-axis: P(CR_α) / P(CR) - 1; y-axis: P(CCR_α) / P(CR) - 1), with α = (b, th15, th60, es, ew, ls, lm, u14, es_u14). 'b' represents a backing wind, 'th15' and 'th60' the weakly and the strongly stably stratified regimes, 'es' and 'ew' the strong and weak wind veer cases with veer over the entire rotor, and 'ls' and 'lm' the strong and moderate wind veer cases with veer limited to the lower rotor part. 'u14' and 'es_u14' represent the cases with an increase of the geostrophic wind.

Fig. 7 it can be concluded that the potential power output of a downwind turbine at 7 D would be larger in case of weak and moderate entrainment of ambient air into the wake. In case of strong entrainment, the difference between counterclockwise and clockwise rotating blades diminishes approaching the 1:1 line. Further, for a weaker mixing in the wake, the potential power output of a downwind turbine decreases in case of clockwise rotating blades (triangles vs. circles). In case of counterclockwise rotating blades (squares vs. circles), the power output of a hypothetical downwind turbine also decreases for decreasing the strength of veer. By changing the atmospheric stratification, the difference for counterclockwise rotating blades is rather small (see Fig. 4(a)), with a slight increase for a stronger stratification corresponding to weaker mixing.

https://doi.org/10.5194/wes-2019-105
Preprint. Discussion started: 28 January 2020

eawe european academy of wind energy
Open Access WIND ENERGY SCIENCE DISCUSSIONS

4 Conclusions

LESs were performed to investigate the rotational direction impact of a wind turbine in a stably stratified ABL flow for veering and backing winds in the NH and the SH. In addition, the difference of a counterclockwise rotating rotor instead of a common clockwise rotating one under veering wind conditions in the NH is investigated for the strength of stratification, the strength and the type of the veering wind and its wind speed.

The paper raises the question: 'Should wind turbines rotate in the opposite direction?'. In the NH, the power increases for counterclockwise rotating blades in comparison to clockwise rotating ones in almost all nighttime configurations with a veering wind investigated in this work. As the simulated conditions are typical for the night (≈10 h a day) and during veered inflow (76% of the nights according to Walter et al. (2009)), and regarding the significant power gain up to 23% under strongly stably stratified conditions and up to 13% under a weakly veering wind the answer 'yes' to this question should seriously be considered for waked wind turbines. In the SH, the situation is directly the opposite due to the different sign of the Coriolis force. Therefore, in the SH, the common clockwise rotational direction of wind turbines is the recommended rotational direction to extract the maximum power when turbines are likely to be waked.

The practicalities of implementing different rotational directions present significant challenges. Choosing opposite rotational directions in the NH and the SH, with changing the current rotational direction in the NH, would have some significant implications for the possibility to share inventory between the wind turbines. For example, the gearbox has many micro-geometry modifications that are based on deformation of the gearbox under loaded conditions. Therefore, it is not possible to make a mirror image gearbox for the NH. It would take a significant amount of modifications to gear tooth profiles, etc., to allow the gearbox to be used in a turbine that rotates in the opposite direction in the NH (John Bosche (ArcVera), personal communication, 2019).

As the results show a significant improvement of wind conditions for a hypothetical downwind turbine by changing the rotational direction of the blades in the NH, it would have a large impact on the produced power (up to 23% difference with the conditions applied in this work), considering the cumulative installed wind capacity in 2017 of 516497 MW (96%) in the NH (Asia, Europe, North America, Africa and Middle East) compared to 539581 MW world wide (GWEC, 2018). Therefore, the market on the NH could be large enough to justify designing a special turbine for the NH, including mirrored blades, gearbox etc. In the SH, the preferential rotational direction is clockwise, and therefore the common wind turbines should result in the maximum produced power at night.

Concluding, a possible extraction of more energy from wind turbines in the NH by simply changing the rotational direction of the blades, could be taken into account in the future.

Author contributions. All authors designed the idea. A. Englberger performed the simulations and prepared the manuscript with contributions from both co-authors.

https://doi.org/10.5194/wes-2019-105
Preprint. Discussion started: 28 January 2020

eawe european academy of wind energy
Open Access WIND ENERGY SCIENCE DISCUSSIONS

Competing interests. The authors declare that they have no conflict of interest.

Acknowledgements. The authors gratefully acknowledge the Gauss Centre for Supercomputing e.V. (www.gauss-centre.eu) for funding this project by providing computing time on the GCS Supercomputer SuperMUC at Leibniz Supercomputing Centre (LRZ, www.lrz.de).

https://doi.org/10.5194/wes-2019-105
Preprint. Discussion started: 28 January 2020

eawe european academy of wind energy
Open Access WIND ENERGY SCIENCE DISCUSSIONS

References

Abkar, M. and Porté-Agel, F.: The effect of atmospheric stability on wind-turbine wakes: A large-eddy simulation study, in: Journal of Physics: Conference Series, vol. 524, p. 012138, IOP Publishing, https://doi.org/10.1088/1742-6596/524/1/012138, 2014.

Abkar, M., Sharifi, A., and Porté-Agel, F.: Wake flow in a wind farm during a diurnal cycle, Journal of Turbulence, 17, 420–441, https://doi.org/10.1080/14685248.2015.1127379, 2016.

Bak, C., Zahle, F., Bitsche, R., Kim, T., Yde, A., Henriksen, L. C., Hansen, M. H., Blasques, J. P. A. A., Gaunaa, M., and Natarajan, A.: The DTU 10-MW reference wind turbine, in: Danish Wind Power Research 2013, 2013.

Bhaganagar, K. and Debnath, M.: Implications of Stably Stratified Atmospheric Boundary Layer Turbulence on the Near-Wake Structure of Wind Turbines, Energies, 7, 5740–5763, https://doi.org/10.3390/en7095740, 2014.

Blay-Carreras, E., Pino, D., Vilà-Guerau de Arellano, J., van de Boer, A., De Coster, O., Darbieu, C., Hartogensis, O., Lohou, F., Lothon, M., and Pietersen, H.: Role of the residual layer and large-scale subsidence on the development and evolution of the convective boundary layer, Atmos Chem Phys, 14, 4515–4530, https://doi.org/10.5194/acp-14-4515-2014, 2014.

Bodini, N., Lundquist, J. K., and Kirincich, A.: US East Coast Lidar Measurements Show Offshore Wind Turbines Will Encounter Very Low Atmospheric Turbulence, Geophysical Research Letters, 46, 5582–5591, https://doi.org/10.1029/2019GL082636, 2019.

Englberger, A. and Dörnbrack, A.: Impact of Neutral Boundary-Layer Turbulence on Wind-Turbine Wakes: A Numerical Modelling Study, Boundary-Layer Meteorology, 162, 427–449, https://doi.org/10.1007/s10546-016-0208-z, 2017.

Englberger, A. and Dörnbrack, A.: Impact of the diurnal cycle of the atmospheric boundary layer on wind-turbine wakes: a numerical modelling study, Boundary-layer meteorology, 166, 423–448, https://doi.org/10.1007/s10546-017-0309-3, 2018a.

Englberger, A. and Dörnbrack, A.: A Numerically Efficient Parametrization of Turbulent Wind-Turbine Flows for Different Thermal Stratifications, Boundary-layer meteorology, 169, 505–536, https://doi.org/10.1007/s10546-018-0377-z, 2018b.

Englberger, A. and Lundquist, J. K.: How does inflow veer affect the veer of a wind-turbine wake?, in: North American Wind Energy Academy 2019 Symposium, Virginia Tech, 2019.

Englberger, A., Dörnbrack, A., and Lundquist, J. K.: Does the rotational direction of a wind turbine impact the wake in a stably stratified atmospheric boundary layer?, Wind Energy Science Discussions, 2019, 1–24, https://doi.org/10.5194/wes-2019-45, https://www.wind-energ-sci-discuss.net/wes-2019-45/, 2019.

Fleming, P., King, J., Dykes, K., Simley, E., Roadman, J., Scholbrock, A., Murphy, P., Lundquist, J. K., Moriarty, P., Fleming, K., et al.: Initial results from a field campaign of wake steering applied at a commercial wind farm–Part 1, Wind Energy Science, 4, 273–285, https://doi.org/10.5194/wes-4-273-2019, 2019.

Gaumond, M., Réthoré, P.-E., Ott, S., Pena, A., Bechmann, A., and Hansen, K. S.: Evaluation of the wind direction uncertainty and its impact on wake modeling at the Horns Rev offshore wind farm, Wind Energy, 17, 1169–1178, 2014.

GWEC, G. W. S.: Global wind statstics 2017, FEBRUARY, 2018.

Hu, H., Yuan, W., Ozbay, A., and Tian, W.: An experimental investigation on the effects of turbine rotation directions on the wake interference of wind turbines, in: 51st AIAA Aerospace Sciences Meeting including the New Horizons Forum and Aerospace Exposition, p. 607, 2013.

Kumar, P. S., Abraham, A., Bensingh, R. J., and Ilangovan, S.: Computational and experimental analysis of a counter-rotating wind turbine system, 2013.

Maegaard, P., Krenz, A., and Palz, W.: Wind power for the world: the rise of modern wind energy, Jenny Stanford, 2013.

https://doi.org/10.5194/wes-2019-105
Preprint. Discussion started: 28 January 2020

Manwell, J., McGowan, J., and Roger, A.: Wind Energy Explained: Theory, Design and Application, Wiley: New York, NY, USA, 134 pp, 2002.

Margolin, L. G., Smolarkiewicz, P. K., and Sorbjan, Z.: Large-eddy simulations of convective boundary layers using nonoscillatory differencing, Phys D Nonlin Phenom, 133, 390–397, https://doi.org/10.1016/S0167-2789(99)00083-4, 1999.

Mühle, F., Adaramola, M. S., and Sætran, L.: The effect of rotational direction on the wake of a wind turbine rotor–a comparison study of aligned co-and counter rotating turbine arrays, Energy Procedia, 137, 238–245, https://doi.org/10.1016/j.egypro.2017.10.346, 2017.

Prusa, J. M., Smolarkiewicz, P. K., and Wyszogrodzki, A. A.: EULAG, a computational model for multiscale flows, Computers & Fluids, 37, 1193–1207, https://doi.org/10.1016/j.compfluid.2007.12.001, 2008.

Sanchez Gomez, M. and Lundquist, J. K.: Influence of wind veer on wind turbine power production, Wind Energy Science, 2019.

Sanderse, B.: Aerodynamics of wind turbine wakes, Energy Research Center of the Netherlands (ECN), ECN-E–09-016, Petten, The Netherlands, Tech. Rep, 5, 153, 2009.

Schmidt, H. and Schumann, U.: Coherent structure of the convective boundary layer derived from large-eddy simulations, J Fluid Mech, 200, 511–562, https://doi.org/10.1017/S0022112089000753, 1989.

Shapiro, A. and Fedorovich, E.: Analytical description of a nocturnal low-level jet, Quarterly Journal of the Royal Meteorological Society, 136, 1255–1262, 2010.

Shen, W. Z., Zakkam, V. A. K., Sørensen, J. N., and Appa, K.: Analysis of counter-rotating wind turbines, in: Journal of Physics: Conference Series, vol. 75, p. 012003, IOP Publishing, https://doi.org/10.1088/1742-6596/75/1/012003, 2007.

Smolarkiewicz, P. K. and Margolin, L. G.: MPDATA: A Finite-Difference Solver for Geophysical Flows, J Comput Phys, 140, 459–480, https://doi.org/10.1006/jcph.1998.5901, 1998.

Smolarkiewicz, P. K., Sharman, R., Weil, J., Perry, S. G., Heist, D., and Bowker, G.: Building resolving large-eddy simulations and comparison with wind tunnel experiments, J Comput Phys, 227, 633–653, https://doi.org/10.1016/j.jcp.2007.08.005, 2007.

Stull, R. B.: An Introduction of Boundary Layer Meteorology, Dordrecht, Kluwer Academic, 1988.

Vermeer, L., Sørensen, J. N., and Crespo, A.: Wind turbine wake aerodynamics, Progress in aerospace sciences, 39, 467–510, https://doi.org/10.1016/S0376-0421(03)00078-2, 2003.

Vollmer, L., Steinfeld, G., Heinemann, D., and Kühn, M.: Estimating the wake deflection downstream of a wind turbine in different atmospheric stabilities: An LES study, Wind Energy Science, 1, 129–141, 2016.

Walter, K., Weiss, C. C., Swift, A. H., Chapman, J., and Kelley, N. D.: Speed and direction shear in the stable nocturnal boundary layer, Journal of Solar Energy Engineering, 131, 011 013, https://doi.org/10.1115/1.3035818, 2009.

Yuan, W., Tian, W., Ozbay, A., and Hu, H.: An experimental study on the effects of relative rotation direction on the wake interferences among tandem wind turbines, Science China Physics, Mechanics & Astronomy, 57, 935–949, 2014.

Zhang, W., Markfort, C. D., and Porté-Agel, F.: Near-wake flow structure downwind of a wind turbine in a turbulent boundary layer, Exp Fluids, 52, 1219–1235, https://doi.org/10.1007/s00348-011-1250-8, 2012.